JOURNAL OF MATERIALS SCIENCE **40** (2005) 1615– 1623

Tensile strength and fracture surface characterisation of sized and unsized glass fibers

S. FEIH*, A. THRANER, H. LILHOLT
Materials Research Department, Risø National Laboratory, Roskilde, Denmark
E-mail: stefanie.feih@risoe.dk

The tensile strength of commercial glass fibers is examined by single fiber tensile tests. The fibers are analysed as received from the manufacturer (sized) and after a heat treatment at 500°C (unsized). Weibull plots of the two series are used for comparison of the strengths of the sized and unsized fibers. It is shown that large sample sizes (over 60 tests) are required to lead to a reliable two-parameter Weibull distribution. The experimental tests clearly indicated that the unsized fibers were weaker in the low strength range, but had similar strength in the high strength range. An investigation of the fracture surfaces in the SEM showed distinct differences in the fracture patterns for high and low strength fibers. Fracture mechanics were applied to estimate the original flaw size and relate the observed fracture mirror surface to the fiber strength. Based on the observation of surface flaws, a "healing" mechanism by the sizing is considered likely for this type of fiber and sizing, thereby effectively increasing the strength of the fiber in the presence of larger surface flaws. © *2005 Springer Science + Business Media, Inc.*

1. Introduction

The manufacture of large structures, i.e., wind turbine rotor blades up to 45 m length or boat hulls, requires a good strength to weight ratio to avoid fracture of the material due to its own weight. Glass fiber reinforced composites are designated materials for these applications. Glass fiber is one of the high performance fibers for composites, and often chosen because of its lower cost in comparison to carbon fiber. However, composite strength in fiber direction is directly influenced by the fiber strength, which shows a large scatter. Fiber strength can be described by the weakest-link theory, which assumes that a given volume of material will fail at the most severe flaw. Size effects occur due to the decreased probability of a smaller volume containing severe flaws. It turns out that such a material is well described by the statistical distribution known as the Weibull distribution [1–4].

Traditionally, glass fibers are coated during production with the so-called fiber sizing, consisting of a water-based formulation of a coupling agent, a film former and other components [5]. The coupling agent is usually a silane-based molecule with reactive ends connecting to the glass and the matrix, respectively. Composite properties can be tailored by modifying the physico-chemical link between fiber and matrix [6], but the entire mechanism of the sizing interaction with fiber and matrix is not yet fully understood.

Optimisation of fiber sizings can require re-sizing and handling of unsized fibers. It is therefore important to consider the effect of sizing on the tensile strength of fibers. While the sizing fulfills the aim of improving the interfacial adhesion between the fibers and the resin, it furthermore protects the fibers during the processing from abrasion and environment [7]. The latter is important, as glass can be susceptible to subcritical crack growth assisted by, for example, moisture from the environment [8]. Zinck *et al*. [2] proposed recently that the application of sizing can "heal" surface flaws of fibers by filling severe flaws with a three-dimensional network of the silane coupling agent, which forms a covalent bond with the glass and thereby effectively reduces the depth of the surface flaw.

In this paper, the strength variation between sized fibers and fibers without sizing (burned off at 500°C) is examined by applying Weibull statistics. The nature of flaws influencing the single fiber strength is determined by characterising the fracture surfaces in the scanning electron microscope (SEM). Glass shows characteristic fracture markings after failure [9, 10]. These fracture characteristics have also been observed for optical fibers with large diameters of the order 100–200 μm [11] and for fiber breakage within ceramic composites [12]. By using information regarding the type of fracture, we can increase the understanding of how the tensile strength of glass fibers is affected by fiber sizing.

*Author to whom all correspondence should be addressed.

TABLE I Fiber specifications

Glass type	E-glass
Fiber diameter (average) (μm)	15.6
Fiber standard deviation (μm)	2.1
Minimum diameter (μm)	10.2
Maximum diameter (μm)	23.4
Type of sizing	Silane
Sizing percentage (wt%)	0.55

2. Experimental method

First, some general information about the fibers is presented. The fibers examined are standard E-glass fibers with specifications as shown in Table I. The large differences in the measured diameters ranging from 10.2 to 23.4 μm emphasise the need of determining the individual fiber diameters prior to each single fiber test. These values in Table I were established by 3-D X-ray synchrotron micro-tomography [13] to examine the cross-sectional areas of the fibers embedded in an epoxy matrix. The high-resolution tomography work with a spatial resolution of 0.7 μm was undertaken by Swiss Light Source, Villingen, Switzerland. The use of tomography results has the advantage that the fiber cross-section is not altered as it normally occurs by polishing the surface for conventional microscopy. The average diameter of 15.6 μm agrees with the manufacturer's specification of 16 μm.

Fibers were tested (1) as received from the manufacturer and (2) after heat treatment of 1 h at 500°C in an oven, followed by cooling down to room temperature. Related research by the authors [6] has shown that this procedure removes most of the sizing layer, with the possibility of small amounts of sizing residues left on the surface.

A cardboard frame (see Fig. 1) with holes stamped at a fixed distance resulted in a gauge length of 20 mm. Single fibers were mounted by applying Impega white tack (re-usable adhesive) at both ends to obtain a vertically positioned fiber on top of this frame with a prestress defined by the weight of the adhesive. The fiber was glued onto the cardboard frame with Loctite 406, as indicated in the figure. The fibers were kept in a plastic bag between measurements to avoid contamination by dust and other particles.

Fig. 1 shows a dotted line, where the holder is cut into two pieces for the strength and diameter measurements, respectively. For the latter, a Leitz Aristomet microscope was used with a magnification of 500X. Each fiber diameter was photographed 10 times at different locations over the length of 20 mm to obtain a meaningful average value and standard deviation along the fiber length. The method of diameter measurement on a separate fiber sample was chosen to avoid damage of the sample used for tensile strength. During handling of the fiber in the microscope, the fiber can be in contact with the objective due to bending of the cardboard and might be scratched.

An Instron tensile test machine (TT-CM) was equipped with a 20 N load cell, which was calibrated to 10 V output for 5 N load due to the low loads expected (typically less than 0.5 N). The cardboard frame was aligned and carefully gripped at the ends to ensure a vertically positioned fiber. Before tensile measurement, the middle piece of the holder was cut away as indicated in Fig. 1. The fibers were tested at a fixed displacement rate of 0.5 mm/min.

For analysis of the fracture surfaces in the SEM, the broken fibers were removed carefully from the cardboard frame and inserted into a sample holder. The holder consisted of two metal blocks with two well-polished surfaces, which could be pressed together by screws. One surface was covered with glue tape to attach the fiber while the two surfaces of the holder were pressed together. Up to five samples were mounted at the same time. It should be noted that the fibers were not allowed to stick more than 50–100 μm out from the sample holder, as sample vibration would cause unstable pictures in the SEM. The fibers and the sample holder were gold-sputtered for 20 s and afterwards investigated in a JEOL 840 SEM under high vacuum. Pictures were taken at a magnification of 5000× and at a voltage of 15 kV.

3. Data analysis

The tensile strength is calculated as follows:

$$\sigma_{\mathrm{TS}} = \frac{F}{A} = \frac{4F}{\pi d^2}, \tag{1}$$

where F is the fracture load and d the measured fiber diameter. The experimental uncertainty was furthermore established to obtain an error estimate for the experiment. The combined uncertainty of the measurement is evaluated as follows [14]

$$\mu_{\mathrm{TS}}^2 = \mu_{\mathrm{F}}^2 + 4\mu_{\mathrm{d}}^2, \tag{2}$$

where the total coefficient of variation on the tensile strength (μ_{TS}) is determined by the coefficient of variation on fracture load (μ_{F}) and diameter (μ_{d}). The coefficient of variation, μ, is obtained be dividing each

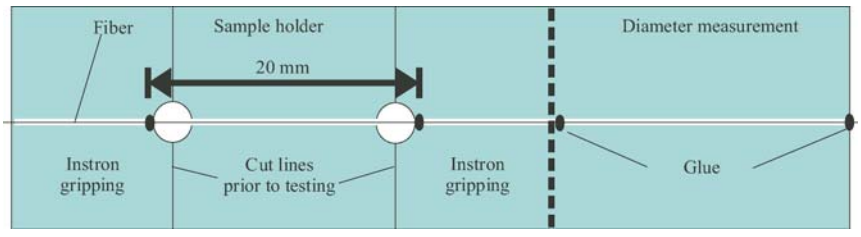

Figure 1 Cardboard frame with fiber resulting in fixed gauge length.

sample standard deviation, s, by its sample mean, $\bar{x}$:

$$\mu = \frac{s}{\bar{x}} \text{ with } \bar{x} = \frac{\sum_{i=1}^{n} x_i}{n} \quad \text{and}$$
$$s = \sqrt{\frac{\sum_{i=1}^{n} (x_i - \bar{x})^2}{n-1}} \tag{3}$$

where x_i indicates the value of the ith measurement and n is the total number of measurements undertaken. Since the diameter measurement contains two sources of uncertainty ((1) along the fiber length, μ_{d1}, and (2) due to the measurement on the "extra piece", μ_{d2}), which are not dependent on each other, μ_d can be determined by adding both values in quadrature as shown in Equation 4.

$$\mu_d = \sqrt{\mu_{d1}^2 + \mu_{d2}^2} \tag{4}$$

The resulting standard deviation, $s_{TS,i}$, which can be evaluated for each strength measurement, $\sigma_{TS,i}$, is as follows:

$$s_{TS,i} = \mu_{TS}\sigma_{TS,i} \tag{5}$$

A statistical analysis of the fiber tensile strength is commonly made by using the two-parameter Weibull distribution [1]. We can write the probability of failure $P_F(\sigma)$ of the fiber at a stress σ and length L as

$$P_F(\sigma, L) = 1 - \exp\left(-\frac{L}{L_0}\left(\frac{\sigma}{\sigma_0}\right)^m\right), \tag{6}$$

where m is the Weibull modulus, σ_0 the characteristic strength and L_0 is the gauge length. The Weibull modulus m is a measure of the scatter in the tensile data. Rearranging the equation above for testing at a fixed gauge length of 20 mm (no volume size effect considered, $L = L_0$), we obtain

$$\ln\left[\ln\left(\frac{1}{1 - P_F(\sigma)}\right)\right] = m\ln\sigma - m\ln\sigma_0. \tag{7}$$

For comparison of the characteristic strength value σ_0 at a different gauge length L_1, Equation 6 can be rewritten as

$$\sigma_0(L_1) = \sigma_0(L_0)\left(\frac{L_0}{L_1}\right)^{1/m}. \tag{8}$$

One arranges the tensile strength values of the fibers in ascending order and assigns a probability of failure using an estimator given by

$$P_F(\sigma_i) = \frac{i - 0.5}{N}, \tag{9}$$

where $P_F(\sigma_i)$ is the probability of failure corresponding to the ith strength value and N is the total number of fibers tested. This expression for the probability of failure is recommended if the Weibull parameters are determined by linear regression [15]. From Equation 7, we can see that the function on the left side varies linearly with $\ln(\sigma)$ and the Weibull modulus is given by the slope, m. It is therefore easy to obtain m and σ_0 by linear regression. The goodness of the linear fit to the Weibull distribution has been used [2] to give an indication of the presence of multiple flaw population, i.e., the presence of surface flaws and/or bulk flaws. The question arises, however, as to how many samples are required to accurately describe and compare a strength distribution with the Weibull distribution. Sample sizes for fiber testing in the literature are reported between 40 [2] and 150 [3] samples. The necessary sample size is discussed in the next Section.

4. Results

To check the reliability of the testing set-up, the Young's modulus was calculated for each single fiber test. The displacement was calculated from the cross head speed of 0.5 mm/min and time, and afterwards divided by the gauge length to obtain the fiber strain. The latter assumes a uniform strain distribution along the fiber. The stress is calculated by dividing the load by the fiber area, which is calculated from the diameter measured for each fiber as described above. The experimental stress-strain curve was linear as expected for brittle fibers. Young's moduli were calculated from the slope of the linear least squares fit. The values are shown in Table II. The average values of 66 GPa are slightly below common values in the literature of about 74 GPa [7]. However, the present calculation of the strain neglects the machine compliance during testing and assumes a gauge length of exactly 20 mm. Both aspects increase the Young's modulus further as (1) the applied displacement decreases if machine compliance is accounted for and (2) the real gauge length increases with deformation of the fiber in the glue area. Nevertheless, the Young's modulus serves as a good experimental check with its current accuracy. No fibers were found during testing that deviated far from the values in Table II as seen by the low standard deviation of the values.

For the uncertainty analysis, the actual value of μ_F could be calculated based on Equation 3 from the individual force measurement, x_F, and a constant value for the standard deviation of $s_F = 0.012$ N as established from the electronic load cell noise. Regarding the diameter measurement uncertainty in Equation 4, μ_{d1} was based on the value for the standard deviation s_{d1} and the corresponding average diameter, $\bar{x}_{d1}$, from the 10 measurements on the extra fiber piece. The value of μ_{d2} was established by correlating measured diameters of 10 fibers with the diameter at a distance of 20 mm along the same fiber, which corresponds to the distance between extra piece and fiber in the sample holder in Fig. 1. A constant value was established

TABLE II Young's moduli as determined from stress-strain curves

	Young's modulus (GPa)	Std. deviation (GPa)
Sized fibers	65.6	4.8
Unsized fibers	66.9	5.3

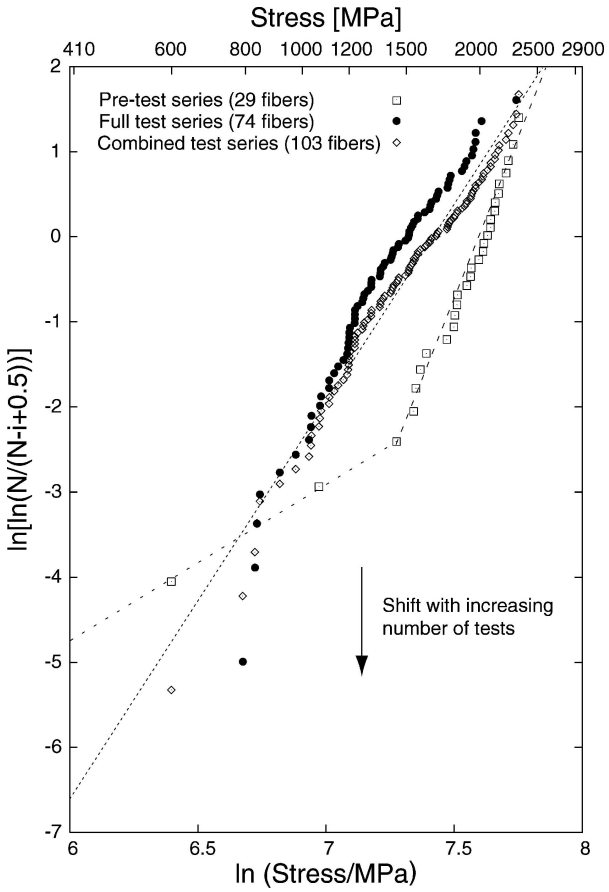

Figure 2 Weibull plot for sized fibers to determine the necessary batch size.

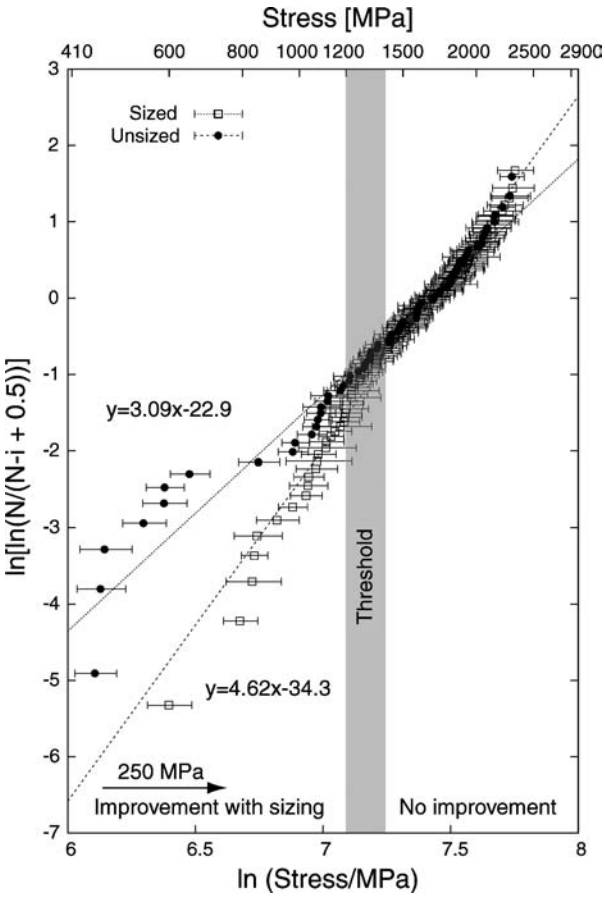

Figure 3 Weibull plot comparison between sized and unsized fibers (error bars indicate the combined measurement uncertainty).

for the coefficient of variation with $\mu_{d2} = 1.8\%$. The relatively small coefficient of variation shows that the fiber diameter does not vary largely along a given fiber, although large diameter variations are found between different fibers (see Table I). The resulting error bars in Fig. 3 correspond to the value of $\pm$ one standard deviation s_{TS} according to Equation 5.

Weibull plots according to Equation 7 of the sized fibers are given in Fig. 2. The distribution with square markers is a pre-testing examination of 29 fibers to establish the testing method, and the distribution with circle markers is an additional data set of 74 tested fibers from the same glass fiber bobbin. As can be seen, the plot for 29 fibers does not give a straight line, although the maximum and minimum strength values for both series are similar. The larger series of 74 fibers, on the other hand, results in a mostly straight line. Comparison of both curves shows that by random selection more high strength than low strength fibers (only two data points describe the lower end of the curve) were evaluated during the pre-test series. It therefore became clear that 29 fibers were not a sufficient number to give reliable strength results. However, if both sets are combined to one data set containing 103 fibers, the line nearly coincides with the full test series, which means that no additional information is gained by adding more test samples. It was therefore decided to use around 75 samples for the unsized fibers.

The difference between the unsized and the sized fibers is presented in Fig. 3. Both the sized and unsized fibers have very similar high strength values, while there are clear differences to be seen in the low strength region. A threshold value of about 1200–1400 MPa is indicated, above which the application of sizing does not seem to improve the fiber strength. The difference in scatter between low and high strength is reflected in the Weibull slopes, $m_{sized} = 4.6$ and $m_{unsized} = 3.1$, of the linear curve fitting equation, while σ_0 is very similar for both systems. Table III shows the resulting Weibull parameters for the sized and unsized fibers. Both fiber types show very good agreement with a linear fit as established by the R^2 curve fit value, which points towards one type of flaw population causing fiber failure. Comparison of the sized fiber values with typical values in the literature for similarly sized glass fibers [3] shows very good agreement as shown in Table III. The volume size effect was accounted for according to Equation 8. It should furthermore be noted that an evaluation of the Weibull parameters with the probability $P_f = i/(N + 1)$ instead of Equation 9 or by applying the maximum likelihood method does not change the parameters significantly.

TABLE III Weibull parameters of the sized and unsized fibers (R^2: statistical evaluation of quality of least squares fit; L: gauge length)

Fiber treatment	m	σ_0 (MPa)	L (mm)	R^2
Sized	4.62	1680	20.0	0.98
Unsized	3.09	1649	20.0	0.96
Sized	4.62	2153 (Equation 8)	6.35	–
APS-sized [3]	3.75	2220	6.35	–

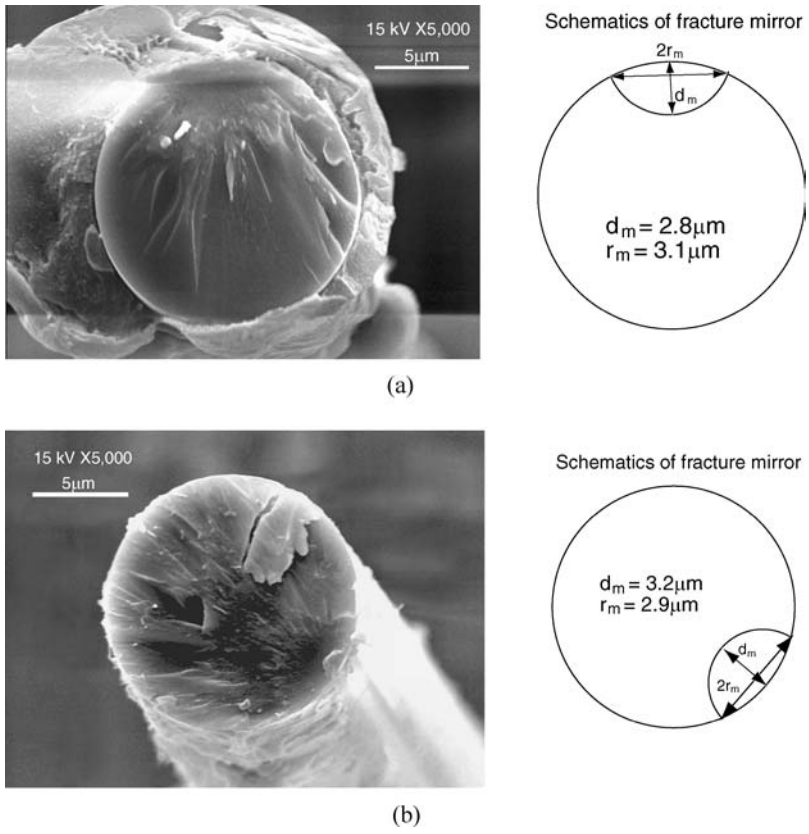

Figure 4 Low strength fracture surface.

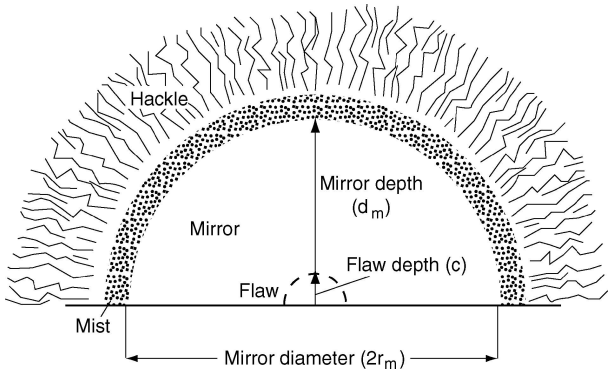

Figure 5 Schematic showing of typical glass surface features that form during failure.

Fracture surface evaluation was undertaken for selected fibres. The fibers were divided into low, medium and high strength ranges. Characteristic, and very different, fracture patterns were observed for low strength and high strength fibers. The typical fracture pattern for low strength fibers can be sketched in Fig. 4 for two samples. It can easily be observed that fracture seems to originate from one side of the fiber as indicated by the fracture mirror with smoother surface. From this point, fracture patterns cross the remaining fiber diameter. These observations are identical with the characteristic fracture surface markings in glass after failure from surface flaws. During failure from an initial, small surface flaw of length c, the crack front propagates through the material, creating fracture features known as the mirror, mist and hackle as seen in Fig. 5 [10, 11]. The crack front initially produces the smooth mirror region. As the crack accelerates, it becomes unstable, thereby creating a dimpled surface known as mist. This instability eventually causes the crack to branch out, producing the rough hackle region. The hackle region is characterised by elongated markings that proceed in the direction of crack propagation and point back to the flaw origin. The measurements of the fracture mirrors are also indicated in Fig. 4. A mist region could not be observed at this scale. The same fracture pattern was observed for **all** low strength fibers (with and without sizing) and some medium strength fibers. Matching patterns on fiber ends originating from the same fiber were furthermore observed.

For high strength fibers on the other hand, two basic types of failure pattern were identified. Fig. 6 visualises the first type of two-plane fracture, which was seen most frequently. Fiber fracture again originated from a point on the surface as indicated by the visible hackle region. Fracture mirrors were only observed on some fracture surfaces (for example Fig. 6a, but not b). After propagating through most of the fiber cross-section, the crack continued at an angle: a second failure plane was created. This could be caused by a more dynamic crack development due to higher strain energy. All fracture mirror measurements are summarised in Table IV. The second type of failure, on the other hand, showed smooth fiber breakage without any indication of a surface fault. Fig. 7 visualises the smooth failure surface for two samples. Unfortunately, it was not possible to confirm that we were indeed looking at the original fracture surface for these high strength fibers with smooth fracture patterns because no matching fiber pair was available during investigation. This is due to

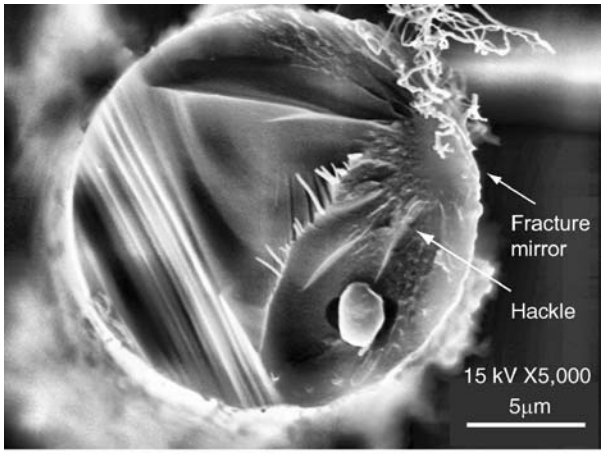

(a)

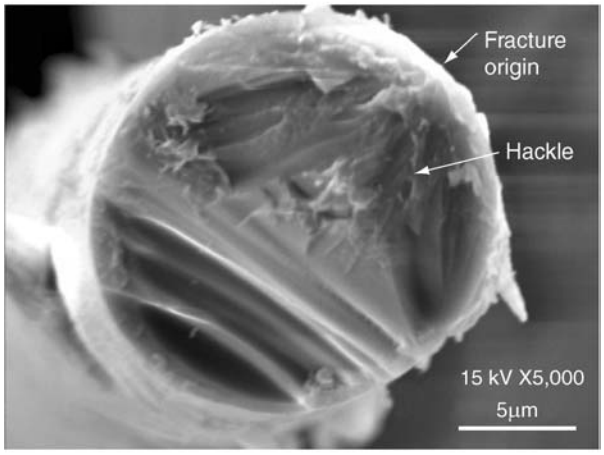

(b)

Figure 6 Two plane failure pattern for high strength fibers.

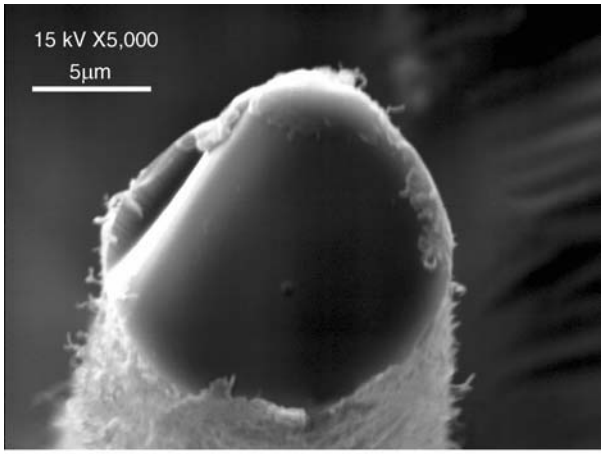

(a)

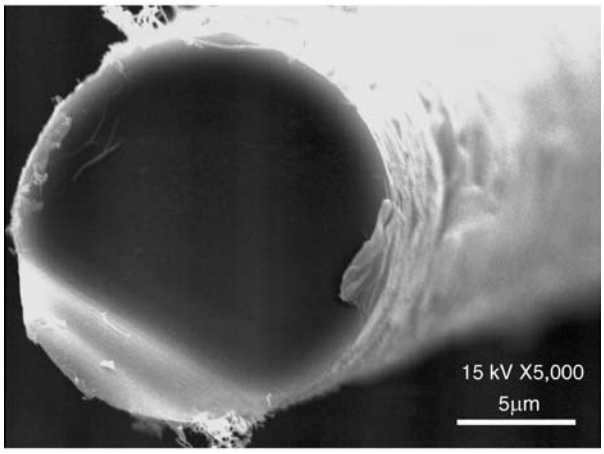

(b)

Figure 7 Smooth failure pattern of high strength fibers.

frequent break-off of fibers from the card board frame after testing. The fracture surfaces could therefore well be a result of secondary breaks caused by bending of the fiber during fracture.

The size of the fracture mirror relates to the pre-existing flaw size and, consequently, the strength of the fiber [12]. Fracture mirror dimensions according to Fig. 4 were observed and measured on eleven fracture surfaces. The mirrors all have circular shapes, and the resulting values for mirror radius and depth (for a definition see Fig. 5) were given in Table IV. It can be seen

TABLE IV Observed mirror dimensions.

Fiber	Fiber strength (MPa)	Mirror radius (r_m) (μm)	Mirror depth (d_m) (μm)
US25	649	2.9	3.2
US05	809	3.1	2.8
S66	995	3.3	7.5
US17	1166	2.8	2.5
US40	1288	3.0	4.2
S75	1292	3.5	3.1
US38	1340	2.6	3.1
S40	1391	3.2	4.0
S28	1735	2.1	3.0
S09	1779	1.7	1.5
US08	1961	1.8	1.6

S: sized fiber, US: unsized fiber.

that higher strength fibers have smaller fracture mirror dimensions.

It has been demonstrated [9–11] that the product of fiber strength and the square root of the mirror radius r_m is constant in silicate glasses:

$$\sigma_{TS} = A_m (r_m)^{-1/2}, \tag{10}$$

where A_m is the so-called mirror constant. For optical glass fibers, the mirror depth d_m instead of the mirror radius has been shown to lead to better least square fitting of the mirror constant especially for larger mirror sizes with up to 90% of the fiber cross-sectional area [11]. This is due to the fact that large fracture mirrors on fiber cross-sections can deviate from the semi-circular shape. Table IV also indicates that the mirror depth and mirror radius are considerably different in our case.

Fig. 8 shows the values of the failure stress plotted versus the reciprocal square root of the mirror depth. The mirror depth was chosen to describe the size of the mirror, as it resulted in better consistency for the mirror constants according to Equation 10 with enforcing the zero point for the linear fit ($A_m = 2.22$ MPa m$^{1/2}$) and without ($A_m = 1.87$ MPa m$^{1/2}$). The least squares fit is not overly satisfactory ($R^2 \approx 0.35$); however, the fitted value for the mirror constant lies well within the range of 1.8–2.5 MPa m$^{1/2}$ reported in the literature for

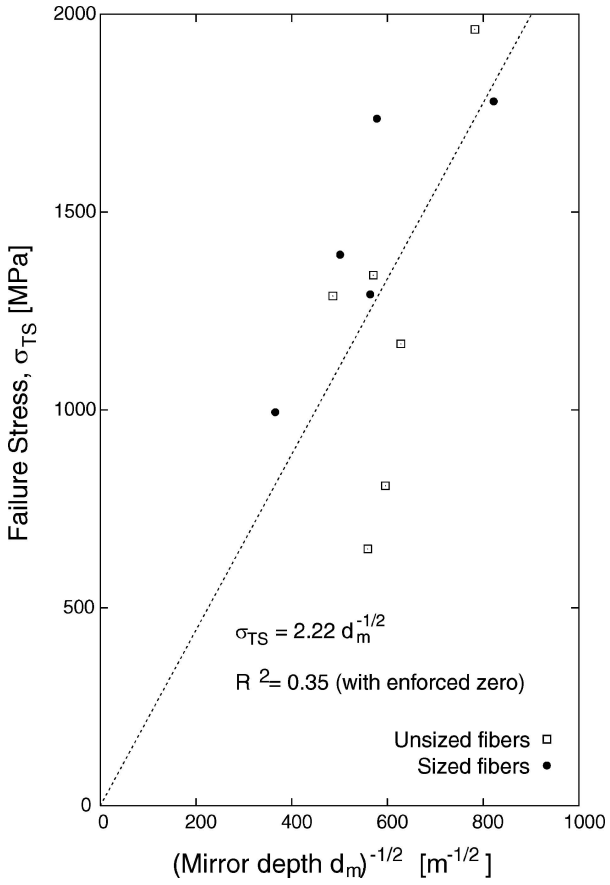

Figure 8 Fracture stress versus reciprocal square roots of mirror depths with least-squares linear fit through the zero point.

glasses [10] and optical glass fibers [11]. It is therefore likely that the relationship between fracture mirror and failure stress (Equation 10) also applies in the case of a very small cross-sectional fracture area.

5. Discussion

The results indicate that the heat treatment, which is well below the glass transition temperature of around 800°C, does not alter the material strength significantly, as a structural change of the glass should lead to a shift of the complete strength range for the heat-treated, unsized fibers. The change in fiber strength in the low strength range must therefore be attributed to the removal of the sizing layer.

As shown in the previous section, low strength fracture is indeed caused by surface flaws, which was established from the typical fracture pattern on the fracture surface. The decrease in strength could be an effect of subcritical crack growth after sizing removal. However, that would most likely affect all cracks, i.e., cause a strength decrease for all fibers. This is not consistent with the experimental results in Fig. 3.

Zinck *et al*. [2] proposed that the application of sizing can "heal" surface flaws of fibers by filling severe flaws with the silane coupling agent. By chemical surface analysis, Wang and Jones [16] confirmed a silane structure based on three layers on the glass surface. These layers consist of (1) an "interfacial" layer, which is covalently bound to the glass surface and remains grafted after a hot water or solvent extraction, (2) a chemisorbed threedimensional layer of polysiloxane and (3) a physisorbed layer of oligomers (non-covalently bound macromolecular aggregates of the silane coupling agent). These layers can alter the effect of surface flaws by filling up part of the cracks as proposed in Fig. 9a, but the synergetic effect depends on the original depth and shape of the surface flaw.

Zinck *et al*. [2] also introduced the concept of a critical threshold flaw size, below which defects are not healed. The existence of a critical threshold explains the similar high strength of both fiber treatments as the existent surface flaws become simply too small to be effectively filled by the molecules of the silane coupling agent (see Fig. 9a). Chemically, the threshold size is then related to the hydrodynamic radius. The hydrodynamic radius describes the size of a molecule and must be smaller than the surface flaw. Previous research by the authors established the presence of an amino-containing silane coupling agent on the fiber, together with an bisphenol-A based epoxy film former, and various other sizing components [6]. Aminofunctional silanes are special as they dissolve instantaneously in aqueous solutions, and form oligomers already at very low weight percentages of around 0.15 wt%, which is important to consider as silanes are normally applied to the fibers from very dilute aqueous solutions. For hydrolysed γ-APS, the most typical amino-containing silane coupling agent, the hydrodynamic radius was established to peak around 150 nm in a weak solution, and attributed to aggregates of smaller molecules rather than inseparable molecular species [17].

Fracture mechanics are applied in the following to firstly determine the shapes of the surface flaws present more closely, and to secondly establish the size of the flaws present in the tested fibers. The chemical

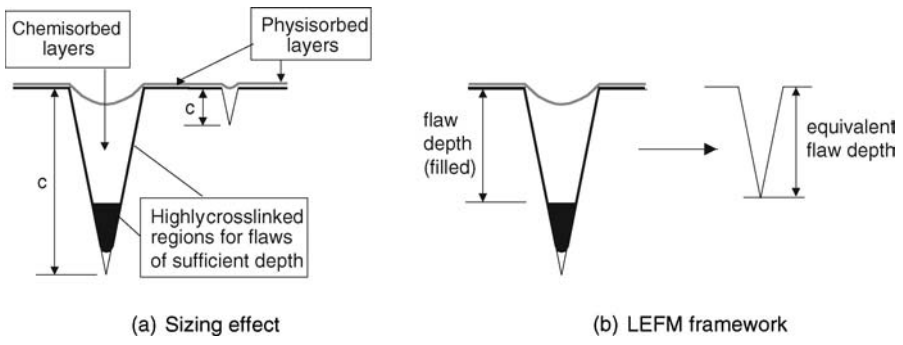

Figure 9 (a) Filling of severe surface flaws by fiber sizing [2] and (b) treatment in the framework of linear elastic fracture mechanics.

threshold value required for the "healing" effect by the silane coupling agent was established to around 150 nm for surface flaws based on the hydrodynamic radius. The crack shape should furthermore relate to the strength threshold value as established from the Weibull plot in Fig. 3.

Planar cracks perpendicular to the fiber axis are the simplest idealisation of the flaw shape present in fibers. The problem can then be solved with a 2-dimensional linear elastic fracture mechanics approach. For a sharp surface flaw, where the flaw size is not considered small compared to the radius of the glass fiber R, the strength σ_{TS} and the flaw depth, c, are related by

$$\sigma_{TS} = \frac{1}{Y(c, R)} K_{IC} (\pi c)^{-1/2}, \qquad (11)$$

where $Y(c, R)$ is a factor depending on the crack geometry and its size in relation to the fiber radius, and K_{IC} is the critical stress intensity factor appropriate for brittle fracture. The latter depends on the material only, and a typical value for borosilicate glass is given with $K_{IC} = 0.76$ MPa $m^{1/2}$ [18]. For the simplified cases of a semi-circular flaw in an infinite body, Y can be considered constant with a value of $Y = 2/\pi$ [19], while for straight surface cracks in an infinite body the factor was determined to $Y = 1.126$ [20]. Levan and Royer [21] derived the dependence of the geometric factor Y as a function of flaw depth c and fiber radius R numerically (see Fig. 10) for these two cases. For small flaws

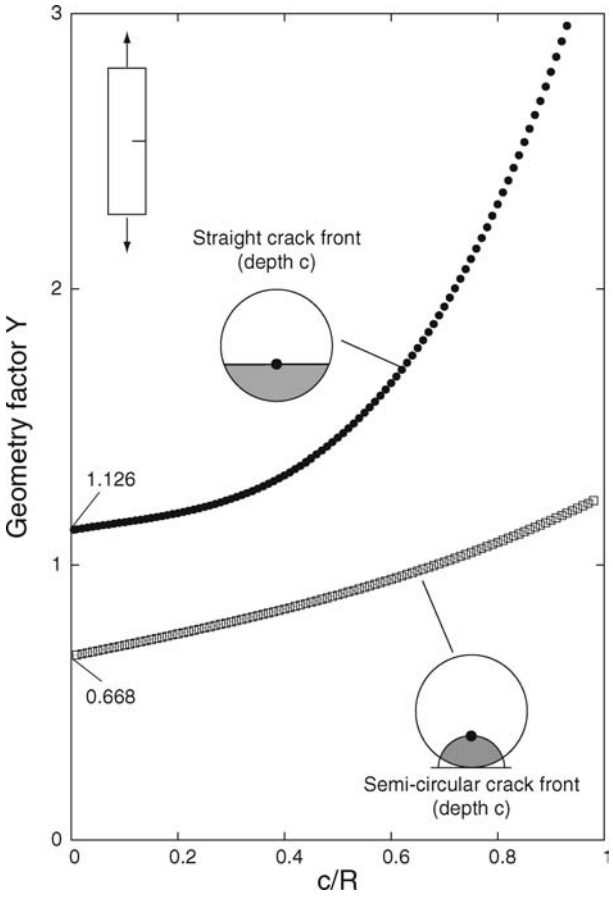

Figure 10 Geometry factor Y in tension at the deepest point for different crack shapes (after Levan and Royer [21]).

TABLE V Calculated flaw depths from strength measurements (depending on flaw geometry)

Strength (MPa)	Semi-circular crack shape		Straight surface crack	
	Y	Flaw depth (nm)	Y	Flaw depth (nm)
1400	0.678	204	1.129	74
1200	0.681	275	1.130	100
700	0.706	753	–	–
450	0.750	1615	–	–

in an infinite body ($c/R \to 0$), the resulting value for semi-circular flaws is about 5% higher than the foregoing analytical value of $2/\pi$, while the numerical value for the straight surface crack agrees very well within an error of 0.4%. This accuracy is found sufficient for the following calculations. The value for Y increases nonlinearly as the size of the flaw increases compared to the fiber radius ($c/R \to 1$).

From Fig. 3, the threshold failure stress for improving the fiber performance due to sizing was established in the range of 1200–1400 MPa. Applying Equation 11 for this strength range yields results of approximately 200–280 nm for the corresponding semi-circular threshold flaw size, c. Assuming straight surface cracks, on the other hand, determines the threshold flaw size to around 75–100 nm, which is considerably lower for the same stress range (see Table V). Considering furthermore that the sizing complexity for the commercial sizing on the fiber is significantly higher due to its variety of components, the filling of surface flaws by the silane coupling agent might be more inhibited. We therefore consider the first threshold flaw size of 200–270 mm for semi-circular flaws to be in better agreement with the chemical considerations, and Equation 11 with the geometry factor Y for semi-circular flaws is applied in the following. Semi-circular flaws, as a result of grinding during surface preparation, have furthermore been observed directly at fracture initiation sites of 3-point bending specimens made from various glass substrates [10].

It is expected that most of flaws were introduced during the fiber manufacture, and are subsequently covered and filled by the sizing. It is therefore of interest to calculate the corresponding flaw depths c to estimate the reduction in flaw depth by the sizing. The fiber strengths in the low strength range in Fig. 3 shift by an average 250 MPa. To find the largest filling efficiency of the sizing, we consider values in the order of 450 MPa (unsized) and 700 MPa (sized), which correspond to the lowest strengths measured. Equation 11 yields a flaw depth of 1615 nm for the corresponding fiber strength of 450 MPa (see Table V). It should be noted that the geometry factor Y as calculated in Table V starts to play a significant role in the calculations at this flaw size ($c/R \approx 0.2$), and should not be neglected. Applying Equation 11 to calculate the flaw depth for the low strength, but sized fibers of 700 MPa leads to an "equivalent" flaw depth about 750 nm. The term "equivalent" is introduced according to Fig. 9b, as the framework of linear elastic fracture mechanics requires some simplifications: (1) the different material properties of the

filling silane coupling agent network are not considered, (2) only highly cross-linked regions act as crack fillers and (3) the crack is assumed to remain sharp. These simplifications are assumed to play a minor role in the calculation, and the "equivalent" flaw depth can be considered similar to the depth of the filled flaw. It becomes evident that the sizing is able to reduce the maximum flaw depth considerably to nearly half of the original flaw depth. The research undertaken clearly indicates the beneficial effect of the fiber sizing on the surface quality of glass fibers. However, the presence of surface flaws also suggests that reduction in the flaw size, and hence strength improvement of the fibers, is possible by focussing on the processing steps related to the fiber surface.

6. Conclusions

Although the tensile strengths of glass fibers have been studied extensively, this paper provides a clear link between improved fiber strength and surface treatment by direct characterisation of the fracture surfaces after testing.

The fracture surface of the glass fiber ends showed clearly that fracture originated from surface flaws. A Weibull plot of the fiber strength distribution showed similar high strengths for sized and unsized fibers, but a clear decrease in the low strength range for unsized fibers compared to sized fibers. A correlation of the chemical molecule size of the coupling agent and the threshold fiber strength, above which no improvement by surface treatment was achieved, led to the conclusion of semi-circular rather than straight cracks on the fiber surface. Overall, based on the above results, it was found likely for the sizing to fill up severe surface flaws. Linear elastic fracture mechanics determined the reduction of the flaw depth to be around 800 nm for the sized, low strength fibers.

Acknowledgements

The authors would like to thank LM Glasfiber A/S (Torben K. Jacobsen) for financial support and helpful discussions for this project. Thanks also to Bent F. Sørensen for input on the fracture mechanics discussions and Emmanuelle Cendre for evaluation of the tomography data.

References

1. W. WEIBULL, The Royal Swedish Institute for Engineering Research, Stockholm, 1939, No. 151.
2. P. ZINCK, M. F. PAYS, R. REZAKHANLOU and J. F. GERARD, *J. Mat. Sci.* **34** (1999) 2121.
3. T. H. CHENG, F. R. JONES and D. WANG, *Comp. Sci. Techn.* **48** (1993) 89.
4. F. M. ZHAO and N. TAKEDA, *Comp. Part A.* **31** (2000) 1203.
5. P. ZINCK, E. MAEDER and J. F. GERARD, *J. Mat. Sci.* **36** (2001) 5245.
6. S. FEIH, J. WEI, P. K. KINGSHOTT and B. F. SOERENSEN, *Comp. Part A* **36** (2005) 245.
7. P. K. GUPTA, in "Fibre Reinforcements for Composite Materials," edited by A. R. Busnell (Elsevier Science Publishers A.V., 1988) p. 19.
8. S. M. WIEDERHORN, *J. Am. Ceram. Soc.* **50** (1967) 407.
9. E. B. SHAND, *ibid.* **42** (1959) 474.
10. J. J. MECHOLSKY, R. W. RICE and S. W. FREIMAN, *ibid.* **57** (1974) 440.
11. R. J. CASTILONE, G. S. GLAESEMAN and T. A. HANSON, in Proceedings of SPIE 4639 on Optical Fiber and Fiber Component Mechanical Reliability and Testing II, 2002, p. 11.
12. M. D. THOULESS, O. SBAIZERO, L. S. SIGL and A. G. EVANS, *J. Am. Ceram. Soc.* **72** (1989) 525.
13. E. CENDRE, S. FEIH and M. STAMPIONI, in "PSI Scientific Report," (2003) Vol. VII, p. 56.
14. H. W. COLEMAN and W. G. STEELE, in "Experimentation and Uncertainty Analysis for Engineers" (John Wiley and Sons, Inc., 1999) p. 54.
15. A. KHALILI and K. KROMP, *J. Mat. Sci.* **26** (1991) 6741.
16. D. WANG and F. R. JONES, *Surf. Interf. Anal.* **20** (1993) 457.
17. H. ISHIDA, S. NAVIROJ, S. K. TRIPATHY, J. J. FITZGERALD and J. L KOENIG, *J. Pol. Sci. Part B.* **20** (1982) 701.
18. S. M. WIEDERHORN, *J. Am. Ceram. Soc.* **52** (1969) 99.
19. D. A. KROHN and D. P. H. HASSELMAN, *ibid.* **54** (1971) 411.
20. W. T. KOITER, *J. Appl. Mech.* **32** (1965) 237.
21. A. LEVAN and J. ROYER, *Int. J. Fract.* **61** (1993) 71.

Received 27 February
and accepted 8 November 2004